Journal of Power Sources 198 (2012) 303–307

Contents lists available at SciVerse ScienceDirect

Journal of Power Sources

journal homepage: www.elsevier.com/locate/jpowsour

Short communication

Graphitized carbon nanofibers for use as anodes in lithium-ion batteries: Importance of textural and structural properties

Ignacio Cameán [a], Ana B. García [a,*], Isabel Suelves [b], José L. Pinilla [b], María J. Lázaro [b], Rafael Moliner [b]

[a] Instituto Nacional del Carbón, CSIC, Francisco Pintado Fe 26, 33011 Oviedo, Spain
[b] Instituto de Carboquímica, CSIC, Miguel Luesma Castán 4, 50018 Zaragoza, Spain

ARTICLE INFO

Article history:
Received 8 August 2011
Received in revised form
13 September 2011
Accepted 29 September 2011
Available online 5 October 2011

Keywords:
Carbon nanofibers
Graphitic materials
Anodes
Lithium-ion batteries

ABSTRACT

The electrochemical performance as anodes in lithium-ion batteries of graphite-like materials that were prepared by high temperature treatment of carbon nanofibers (CNFs) is investigated by galvanostatic cycling. These CNFs were produced in the catalytic decomposition of methane (CDM). By this process, a valuable free-CO_2 hydrogen was simultaneously produced. The graphitized CNFs have provided reversible capacities up to 320 mA h g^{-1} after 50 discharge/charge cycles. These values are similar to those of oil-derived graphite (petroleum coke being the main precursor) which are currently employed as anode in the commercial lithium-ion batteries. Moreover, they have showed excellent cyclability and cycling efficiency (>99%), thus making feasible their application to this end.

Besides the degree of crystallinity, the presence of loops between adjacent active end planes on the graphene layers of the graphitized CNFs were also found to influence on the battery reversible capacity. The textural properties of these graphitic materials, specifically, the surface area and the mesopore volume, are important factors affecting their performance as anode in terms of irreversible capacity and capacity retention along cycling, respectively.

1. Introduction

Graphite with relatively high specific capacity, high cycling efficiency and low irreversible charge is nowadays the choice of a majority of the commercially available lithium-ion batteries. This type of batteries is currently the energy source for most of the portable electronic devices [1]. Moreover, their global demand is expected to grow due to the manufacturing of the electric vehicles, thus affecting the graphite market both in terms of production and price [2].

The production of graphite involves the selection of carbon materials that graphitize readily. Currently, petroleum coke is used as the main precursor material in the manufacturing of synthetic graphite [3]. Different factors, however, have drawn the researcher interests towards the study of other alternative precursors. Among them, carbon nanofibers (CNFs) from the catalytic decomposition of methane (CDM) were found to graphitize when heated at temperatures above 2400 °C [4]. By this process, free-CO_2 hydrogen is simultaneously produced. Moreover, depending on the catalyst used, the CNFs may contain different metals (Ni, Si, Ti, etc.) which have been traditionally used as graphitization catalysts of carbon materials [5]. Taking advantage of this catalytic effect, graphite-like materials with a very high degree of crystallinity were recently prepared in our laboratory from CNFs [6].

On the basis of these results, the electrochemical performance as potential anodes in lithium-ion batteries of graphitic materials that were obtained by high temperature treatment of CNFs is herein investigated by galvanostatic cycling. The CNFs were produced by CDM in the presence of a nickel-based catalyst. Since good electrode capacity retention is an important requirement for the manufacturing of these batteries, the reversible capacity provided by the materials prepared on prolonged cycling is also studied. The influence of the structural and textural properties of the graphitized CNFs on their anodic behaviour is discussed.

Some studies on the utilization of carbon nanofibers as anodes in lithium-ion batteries have been previously reported [7–16]. In these works, CNFs were prepared from different precursors and processes. However, to the best of our knowledge, the work presented in this paper is the first one showing the electrochemical results of graphitized CNFs that were initially obtained by CDM in which the simultaneous production of a valuable fuel (hydrogen) was also studied [4].

2. Experimental

2.1. Carbon nanofibers preparation

The CNFs were produced in a fluidized bed reactor by CDM at a temperature of 700 °C, a space velocity of 12 N dm^3 CH_4 ($h\ g_{cat}$)$^{-1}$

* Corresponding author. Tel.: +34 985 118954; fax: +34 985 297662.
E-mail address: anabgs@incar.csic.es (A.B. García).

0378-7753/$ – see front matter © 2011 Elsevier B.V. All rights reserved.
doi:10.1016/j.jpowsour.2011.09.103

Table 1
Textural parameters of the graphitized CNFs and of the SG graphite of reference.

Material	S_{BET} ($m^2\ g^{-1}$)[a]	V_t ($cm^3\ g^{-1}$)[b]	V_{MESO} ($cm^3\ g^{-1}$)[c]	V_{MICRO} ($cm^3\ g^{-1}$)[d]
CNF-6/2800	30	0.087	0.078	0.009
CNF-10/2800	32	0.089	0.081	0.008
CNF-15/2800	23	0.068	0.055	0.013
CNF-15/2900	19	0.067	0.061	0.006
SG	3	–	–	–

[a] BET surface area calculated from the N_2 adsorption data.
[b] Total N_2 pore volume (at $p/p^0 = 0.976$).
[c] Mesopore volume obtained by DFT.
[d] Micropore volume = $V_t - V_{MESO}$.

and a reaction time of 7 h. The experimental set up is described in detail elsewhere [17]. A nickel–copper based catalyst prepared by the fusion method using SiO_2 as textural promoter was employed. The catalyst preparation procedure as well as characterization is reported in [18]. Three CNFs denoted as CNF-*X* (*X*: 6, 10 or 15) where *X* corresponds to the wt.% of Si have been studied [6]. They were ground in a planetary ball mill prior heat treatment.

2.2. High temperature treatments of the carbon nanofibers

The graphitization experiments of the CNFs were carried out at 2800 and 2900 °C in a graphite electrical furnace for 1 h under argon flow. The heating rates were 25 °C min^{-1} from room temperature to 1000 °C, 20 °C min^{-1} in the range 1000–2000 °C and 10 °C min^{-1} from 2000 °C to the final temperature. The resulting graphitized materials are identified by including a suffix with the treatment temperature in the carbon nanofibers designations, such as CNF-6/2800. No metallic content was detected in the graphitized CNFs as determined by inductively coupled plasma-optical emission spectroscopy.

2.3. Characterization of the graphitized carbon nanofibers

The interlayer spacing, d_{002}, and the mean crystallite sizes along *c*, L_c, and *a*, L_a, axes are used in this study to asses the degree of structural order of the graphitized carbon nanofibers [19]. They were calculated from the powder X-ray diffractograms which were recorded as reported previously [20]. d_{002} was determined from the position of the (0 0 2) peak by applying the Bragg's equation, while L_c and L_a were calculated from the (0 0 2) and (1 1 0) width peaks, respectively, using the Scherrer formula, with values of $K = 0.9$ for L_c and 1.84 for L_a [21]. The broadening of diffraction peaks due to instrumental factors was corrected with the used of a silicon standard. Typical standard errors of the XRD parameters are <2% and <5% of the reported values for L_c and L_a, respectively; the d_{002} values are much more precise, with standard errors of <0.01%. Raman spectroscopy has been also used to estimate the degree of orientation of the microcrystallites. Raman spectra were obtained in a Raman microspectrometer as described previously [22]. The intensity *I* of the Raman bands was measured using a mixed Gaussian–Lorentzian curve-fitting procedure. The relative intensity of the Raman D-band I_D/I_t ($I_t = I_G + I_D + I_{D'}$) was calculated with standard errors lower than 5%.

The textural properties of the graphitized CNFs were measured by N_2 adsorption–desorption at −196 °C in Micromeritics ASAP 2420 or 2020 volumetric adsorption systems. Before measurements, the samples were degassed overnight at 250 °C. The specific surface areas (S_{BET}) were calculated by applying the Brunauer–Emmett–Teller (BET) method, taking 16.2 nm^2 for the cross-sectional area of the nitrogen-adsorbed molecule. Total pore volumes (V_t) were determined by the amount of N_2 adsorbed at $p/p^0 = 0.97$. Mesopore volumes (2–50 nm) were calculated from the cumulative pore size distributions obtained by applying the DFT (density functional theory) method to the N_2 adsorption isotherms ($p/p^0 = 0.97$). Cumulative pore size distributions are given as supplementary material in Fig. S1.

Transmission electron microscopy (TEM) was carried out on a Jeol 2011 microscope equipped with a LaB_6 gun and operating at 200 kV. The samples were firstly finely grounded, dispersed in ethanol and a drop of solution was then deposited on a classical TEM copper grid, previously covered by a holey amorphous carbon film. Examination of the sample was focused on parts of the samples lying across the holes to obtain information free of the contribution of the supporting carbon film.

2.4. Cell preparation and electrochemical measurements

For the electrochemical measurements, two-electrodes Swagelok-type cells were used. Metallic lithium discs of 12 mm diameter were the counter-electrodes. The working electrodes were prepared by mixing the active material (92 wt.%) and PVDF binder (8 wt.%) in 1-methyl-2-pyrrolidone solution. All of the materials prepared were ground prior the electrode preparation. The suspension was deposited on a copper foil of 12 mm diameter by airbrushing to obtain a thin and uniform surface coating, and then was vacuum dried at 120 °C for 20–24 h. Finally, it was hydraulically pressed at a pressure of 0.9 tn cm^{-2}. Afterwards, the electrode load (active material + binder) and active material content were calculated by weight difference. The electrode load densities were in the range 2.88–4.80 mg cm^{-2}. Glass micro-fiber disks impregnated with 1 M $LiPF_6$ (EC:DEC, 1:1, w/w) electrolyte solution were the electrode separators. All cells were assembled in a dry box under argon atmosphere and water content below 1 ppm. The galvanostatic cycling was carried out in the 2.1–0.003 V potential range at a constant current of *C*/10 (corresponding to a capacity of 372 mA h g^{-1} in 10 h) during 50 cycles versus Li/Li^+, using a potentiostat/galvanostat.

3. Results and discussion

3.1. Structural and textural properties of the graphitized carbon nanofibers

To help in discussing the electrochemical results, the textural (Table 1) and structural properties (Table 2) of the graphitized carbon nanofibers are firstly considered. The BET surface areas of

Table 2
Interplanar distance d_{002}, and crystallites sizes L_c and L_a of the graphitized CNFs and of the SG graphite of reference.

Material	d_{002} (nm)	L_c (nm)	L_a (nm)	I_D/I_t (%)
CNF-6/2800	0.3377	18.0	43.8	32.2
CNF-10/2800	0.3373	21.4	47.1	25.2
CNF-15/2800	0.3364	35.9	50.6	25.5
CNF-15/2900	0.3364	39.6	52.2	30.0
SG	0.3361	50.4	61.1	10.0

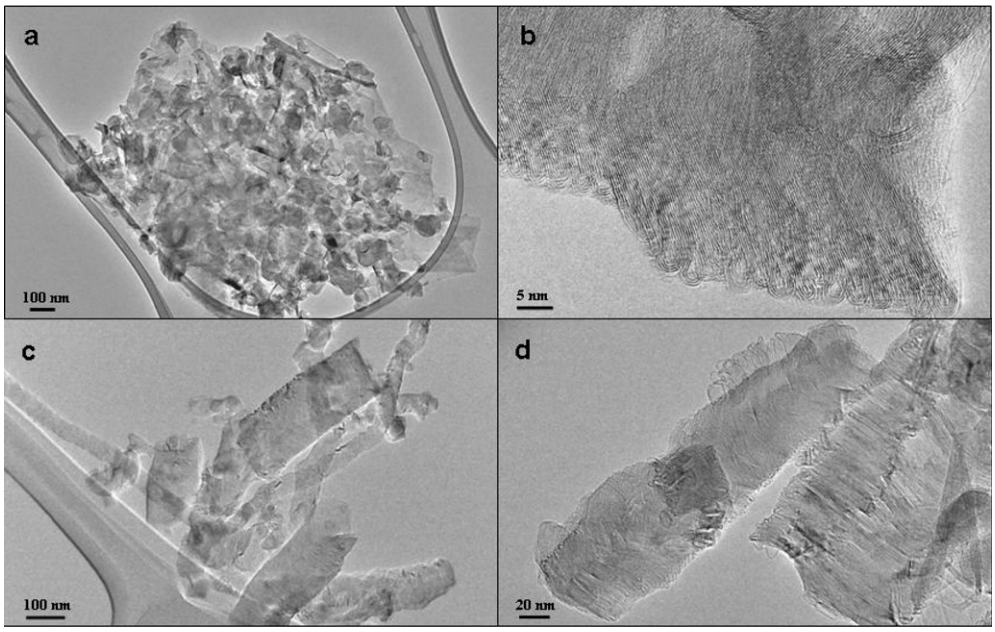

Fig. 1. TEM images of graphitized carbon nanofibers: (a, b) CNF-6/2800 and (c, d) CNF-15/2900.

these materials range from 19 to 32 $m^2\ g^{-1}$ mainly due to the presence of mesopores. The materials porosity follows the sequence CNF-6/2800 ≈ CNF-10/2800 > CNF-15/2900 ≈ CNF-15/2800. A comparative analysis of the cumulative pore volume distributions (Fig. S1) of these nanofibers does not show additional differences as regards the different mesopore size ranges. As seen in Fig. 1, the graphitized CNFs are of various sizes, their morphology being mainly of fishbone type.

The graphitized carbon nanofibers exhibit a high degree of structural order with d_{002} in the range 0.3364–0.3377 nm, and crystallites sizes, L_c and L_a, up to ~40 nm and ~52 nm, respectively. As expected, more crystalline materials were achieved by increasing the treatment temperature of a given CNF (Table 2). However, the Raman I_D/I_t ratio appears larger than that calculated for other non fibers-based graphitic materials with similar XRD parameters [20,22,23]. Furthermore, no variation or even an increase of this ratio was observed by improving the degree of structural order of the graphitized carbon nanofibers (Table 2). The development of a more graphite-like structure is associated with the increase of the G-band (after graphite) and the decrease of the D-band (after defects) intensities of the Raman spectrum [19,24]. Therefore, an I_D/I_t ratio fall was also expected to occur. The formation of loops between adjacent active end planes on the graphene layers of the graphitized CNFs (see HRTEM images in Fig. 1) can account for these results. In fact, the presence of loops has been found to affect the Raman spectra of the materials, particularly the intensity of the D′-band [25] which in carbons has been ascribed to end planes [26]. Accordingly, the increase of the CNFs treatment temperature seems to enhance the loops formation, thus explaining the higher I_D/I_t ratio of CNF-15/2900 as compared to that of CNF-15/2800 (Table 2).

By comparing the XRD (Table 2) and textural (Table 1) parameters of the graphitized CNFs, it is evident that the decrease of the BET surface area/pore volume can be associated with the increase of the structural order as a consequence of the growth of the crystallite size and the removal of the graphene layers defects. Moreover, this decrease mainly occurs at the expenses of the mesopores which are located in the nanofibers interior along the axis.

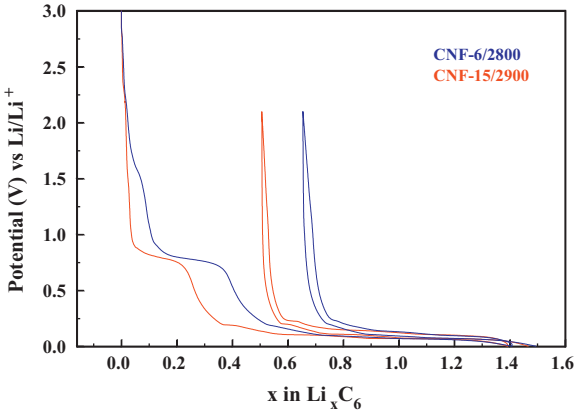

Fig. 2. Galvanostatic first discharge–charge cycle and second discharge profiles of CNF-6/2800 and CNF-15/2900 graphitized carbon nanofibers. (For interpretation of the references to color in this artwork, the reader is referred to the web version of this article.)

3.2. Anodic performance of the graphitized carbon nanofibers: galvanostatic cycling

The mechanism of lithium intercalation into the graphitized carbon nanofibers is typical of graphitic materials; the potential changes showing different plateau regions [27]. As an example, the first discharge–charge cycle and second discharge voltage profiles of the cells using CNF-6/2800 and CNF-15/2900 materials as working electrodes are shown in Fig. 2. During the first discharge process, the cell voltage drops quickly to ~0.8 V (versus Li/Li^+) to form a plateau. This plateau is associated with the solid electrolyte interface (SEI) film formation on the graphite surface as a result of the electrolyte decomposition. With further discharging, the potential decreasing continues to the point at what the lithium intercalation into the graphene layers starts as shown by the appearance of plateaus in the range below 0.2 V. Besides the mentioned plateaus, an additional sloped plateau at higher voltages (~1.8 V) than the SEI formation can be seen in the potential

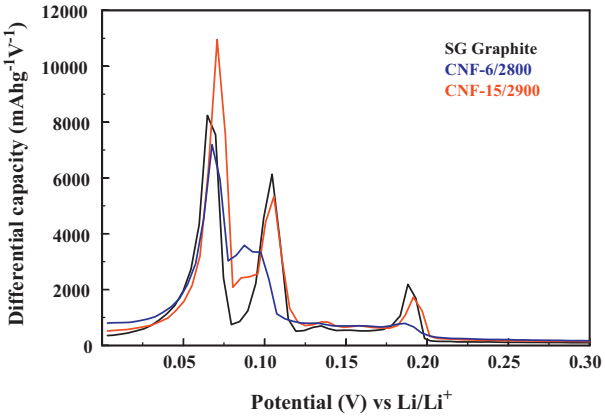

Fig. 3. Differential capacity during the first discharge cycle of CNF-6/2800 and CNF-15/2900 graphitized carbon nanofibers, and of SG graphite of reference. (For interpretation of the references to color in this artwork, the reader is referred to the web version of this article.)

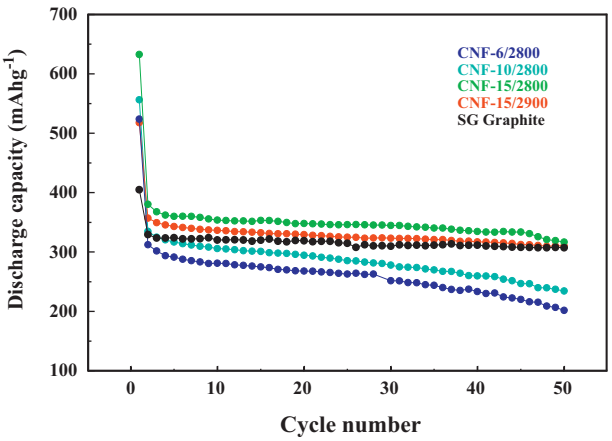

Fig. 4. Extended galvanostatic cycling of the graphitized CNFs and of the SG graphite of reference. (For interpretation of the references to color in this artwork, the reader is referred to the web version of this article.)

versus Li/Li^+ profile of CNF-6/2800 (Fig. 2). It was also observed in CNF-10/2800 with comparable structural and textural properties. This pseudoplateau has been previously ascribed to charge transfer on the surface of the carbon nanofibers [12–14] or related to the Li^+ extraction from defects sites with higher energy in the case of other nano carbon materials [28]. As expected, the lithium storage over the SEI potential was found to decrease significantly in highly graphitized carbon nanofibers [29]. Therefore, during the first discharging cycle of CNF-15/2900, the potential falls vertically to ~0.8 V (Fig. 2). The lithium ions intercalation into the materials can be appreciated better in the differential capacity (absolute value, derived from the first cycle discharge data) versus potential plot in Fig. 3. Data corresponding to SG synthetic graphite was also included in this figure. This graphite – currently commercialized to be employed in the manufacturing of lithium-ion battery anodes – was used as a reference material and its characterization was carried following the same procedures described in the experimental section for the graphitized CNFs. As seen, three main peaks corresponding to the different lithium intercalation stages appear in the profiles of CNF-6/2800 and CNF-15/2900. Nevertheless, the lithium intercalations into the more structurally ordered CNF-15/2900 occur at higher potentials. This trend was previously observed in materials with different degree of graphitization prepared, as here, from the same precursor [30]. Moreover, other peak of very low intensity at ~0.13 V can be noticed in the profiles of CNF-15/2900 and SG. This peak has been assigned to the coexistence of 3 and 2L lithium intercalation stages in graphitic materials with very high degree of crystallinity in which disordered phases are not present [31]. Even though, a comparison of the profiles of CNF-15/2900 and SG in Fig. 3 reveals some differences in lithium intercalation. Specifically, the intensity of the peak at the lowest potential of ~0.06 V is significantly higher in the graphitized carbon nanofiber. Provided similar development of the graphitic structure (Table 2), this difference should be essentially due to the nanometric size of CNF-15/2900 since it has been reported to favour the diffusion of lithium ions into the materials, thus improving their electrochemical performance [32,33].

As compared to other graphitic materials [20], the irreversible charge losses (irreversible capacity, C_{irr}) during the first discharge–charge cycle of the graphitized CNFs is unusually large. It is due to their higher surface area what has been related with this electrochemical parameter [34]. Specifically, irreversible capacities of ~289, ~243, ~299 and ~188 mA h g^{-1} were calculated for CNF-6/2800, CNF-10/2800, CNF-15/2800 and CNF-15/2900, against a value of ~94 mA h g^{-1} for the petroleum-based powder synthetic graphite (SG) with a much lower surface area (3 m^2 g^{-1}, Table 1).

After the SEI formation during this initial cycle, significant differences in the cycling behaviour of the carbon nanofibers studied are observed (Fig. 4). Thus, CNF-15/2800 and CNF-15/2900 provide reversible capacities in the interval 320–310 mA h g^{-1}. They also show a remarkable stable capacity along cycling with capacity keeping values of 83% and 87%, respectively, after 50 cycles and cycling efficiencies (discharge capacity/charge capacity) >99%. Moreover, the performance as anode on prolonged cycling of these graphitized CNFs compares well with that of the SG graphite of reference studied (Fig. 4). The battery reversible capacity decreases remarkably by using the other two carbon nanofibers (CNF-6/2800, CNF-10/2800) tested as anodes. It is well known that the electrochemical intercalation of lithium in well-ordered (graphite-like) carbon materials depends on their crystal structure [6,20,27,35,36]. Specifically, the crystal thickness, L_c, was reported to be the most important factor affecting the extent of the reversible capacity in graphitic materials providing similar morphology and particle size. Therefore, the smaller capacity provided by CNF-6/2800 and CNF-10/2800 (Fig. 4) can be initially attributed to the much larger L_c values of CNF-15/2800 and CNF-15/2900 (Table 2). Accordingly, parallel evolutions of the carbon nanofibers reversible capacity during cycling should be at first expected. However, this trend was not observed at all. On the contrary, CNF-6/2800 and CNF-10/2800 exhibit very low retention capacity, particularly from the 20th cycle, (a minimum of 57% was calculated for CNF-6/2800 after 50 cycles). For comparison, at the 10th and 50th cycles, CNF-10/2800 supplies 306 and 235 mA h g^{-1} against 337 and 310 mA h g^{-1} reached with CNF-15/2900. Despite their poorer cycling performance, CNF-6/2800 and CNF-10/2800 nanofibers also show a cycling efficiency > 99%. Therefore, the continuous battery capacity loss when cycling these nanofibers cannot be due to lithium ions irreversible trapped inside the pores/cavities since their intercalation is basically reversible. In consequence, it is likely that the graphitic structure of CNF-6/2800 and CNF-10/2800 is progressively damaged, particularly from 20th cycle. As previously discussed, these materials have larger mesopore volume in the whole range of sizes (Table 1 and Fig. S1), thus increasing the probability of inserting solvated lithium what leads to the exfoliation of the graphene sheets.

Finally, the reversible capacity provided by CNF-15/2800 is larger than that of CNF-15/2900 with a higher degree of structural order (Table 2 and Fig. 4). The porosity of these two graphitized CNFs is comparable (Table 1). Therefore, the unexpected lower

value of CNF-15/2900 could be associated with the formation of loops between adjacent graphene layers what appears to be more significant in this material (see Section 3.1). The intercalation of the lithium ions into all of the graphene layers available in the graphitized carbon nanofibers can be hampered by the presence of loops [29].

4. Conclusions

The graphite-like materials prepared by high temperature treatment of carbon nanofibers that were obtained in the catalytic decomposition of methane have provided reversible capacities up to ~320 mAh g^{-1} after 50 discharge–charge cycles. These values are similar to those of oil-derived graphite (petroleum coke being the main precursor) which are currently employed as anode in the commercial lithium-ion batteries. Moreover, they have showed excellent cyclability and cycling efficiency, thus making feasible their application to this end. Provided comparable development of the graphitic structure, the nanometric size of the graphitized carbon nanofibers appear to favour the diffusion of the lithium ions into the materials, thus improving their electrochemical performance.

Besides the degree of crystallinity, the presence of loops between adjacent active end planes on the graphene layers of the graphitized carbon nanofibers were also found to influence on the battery reversible capacity. Moreover, the textural properties of these materials, specifically, the surface area and the mesopore volume, are important factors affecting their performance as anode in terms of irreversible capacity and capacity retention along cycling, respectively.

Acknowledgements

Financial support from the Spanish Ministry of Science and Innovation MICINN (under Project ENE2008-06516) is gratefully acknowledged. Thanks are due to Prof. J. N. Rouzaud for helping in the TEM characterization.

Appendix A. Supplementary data

Supplementary data associated with this article can be found, in the online version, at doi:10.1016/j.jpowsour.2011.09.103.

References

[1] M. Wakihara, Mater. Sci. Eng. R33 (2001) 109.
[2] D.W. Olson, Graphite, 2006 Mineral Year Book, U.S. Geological Survey, U.S. Department of Interior, Washington, 2007.
[3] M. Inagaki, Applications of polycrystalline graphite, in: P. Delhaès (Ed.), Graphite and Precursors, Gordon and Breach, Amsterdam, 2001, pp. 179–198.
[4] A.B. Garcia, I. Cameán, I. Suelves, J.L. Pinilla, M.J. Lázaro, J.M. Palacios, R. Moliner, Carbon 47 (2009) 2563.
[5] H. Marsh, A.P. Warburton, J. Appl. Chem. 20 (1970) 133.
[6] A.B. Garcia, I. Cameán, J.L. Pinilla, I. Suelves, M.J. Lázaro, R. Moliner, Fuel 89 (2010) 2160.
[7] V. Subramanian, H. Zhu, B. Wei, J. Phys. Chem. B 110 (2006) 7178.
[8] L. Ji, Y. Yao, O. Topralci, Z. Lin, Y. Liang, Q. Shi, A.J. Medford, C.R. Millns, X. Zhang, J. Power Sources 195 (2010) 2050.
[9] T. Doi, A. Fukuda, Y. Iriyama, T. Abe, Z. Ogumi, K. Nakagawa, T. Ando, Electrochem. Commun. 7 (2005) 10.
[10] S.-H. Yoon, C.-W. Park, H. Yang, Y. Korai, I. Mochida, R.-T.K. Baker, N.M. Rodriguez, Carbon 42 (2004) 21.
[11] J. Zhang, Y.-S. Hu, J.-P. Tessonnier, G. Weinberg, J. Maier, R. Schögl, D.S. Su, Adv. Mater. 20 (2008) 1450.
[12] C. Li, X. Yin, L. Chen, Q. Li, T. Wang, J. Phys. Chem. C 113 (2009) 13438.
[13] J. Zhou, H. Song, B. Fu, B. Wu, X. Chen, J. Mater. Chem. 20 (2010) 2794.
[14] D. Deng, J.Y. Lee, Chem. Mater. 19 (2007) 4198.
[15] G. Zou, D. Zhang, C. Dong, H. Li, K. Xiong, L. Fei, Y. Qian, Carbon 44 (2006) 828.
[16] M. Endo, Y.A. Kim, T. Hayashi, K. Nishimura, T. Matusita, K. Miyashita, M.S. Dresselhaus, Carbon 39 (2001) 1287.
[17] J.L. Pinilla, R. Moliner, I. Suelves, M.J. Lázaro, Y. Echegoyen, J.M. Palacios, Int. J. Hydrogen Energy 32 (2007) 4821.
[18] M.J. Lázaro, Y. Echegoyen, I. Suelves, J.M. Palacios, R. Moliner, Appl. Catal. A: Gen. 329 (2007) 22.
[19] A. Cuesta, R. Dhamelincourt, R. Laureyns, A. Martínez-Alonso, J.M.D. Tascón, J. Mater. Chem. 8 (1998) 2875.
[20] I. Cameán, A.B. Garcia, J. Power Sources 196 (2011) 4816.
[21] J. Biscoe, B.J. Warren, J. Appl. Phys. 13 (1942) 364.
[22] I. Cameán, P. Lavela, J.L. Tirado, A.B. Garcia, Fuel 89 (2010) 986.
[23] M. Cabielles, M.A. Montes-Morán, A.B. Garcia, Energy Fuels 22 (2008) 1239.
[24] A. Cuesta, R. Dhamelincourt, R. Laureyns, A. Martínez-Alonso, J.M.D. Tascón, Carbon 32 (1994) 1523.
[25] K. Fujisawa, T. Hasegawa, D. Shimamoto, H. Muramatsu, Y.C. Jung, T. Hayashi, Y.A. Kim, M. Endo, ChemPhysChem 11 (2010) 2345.
[26] G. Katagiri, H. Ishida, A. Ishitani, Carbon 26 (1988) 565.
[27] M. Endo, C. Kim, K. Nishimura, T. Fujino, K. Miyashita, Carbon 38 (2000) 183.
[28] J. Hu, H. Li, X. Huang, Solid State Ionics 178 (2007) 265–271.
[29] H. Habazaki, M. Kiriu, H. Cono, Electrochem. Commun. 8 (2006) 1275–1279.
[30] S. Flandrois, B. Simon, Carbon 37 (1999) 165.
[31] T. Zeng, J.R. Dahn, Synth Met. 73 (1995) 1–7.
[32] K.T. Lee, J. Cho, Nano Today 6 (2011) 28–41.
[33] M. Pumera, Energy Environ. Sci. 4 (2011) 668–674.
[34] M. Winter, P. Novak, J. Monnier, J. Electrochem. Soc. 145 (1998) 428–436.
[35] C. Arrebola, A. Caballero, L. Hernán, J. Morales, J. Electrochem. Soc. 156 (2009) A986–A992.
[36] M. Endo, Y. Nishimura, T. Takahasi, K. Takeichi, M.S. Dresselhaus, J. Phys. Chem. Solids 57 (1996) 725–728.